Available online at www.sciencedirect.com

ScienceDirect

Advances in Space Research 63 (2019) 1914–1925

ADVANCES IN SPACE RESEARCH (a COSPAR publication)

www.elsevier.com/locate/asr

The longitudinal and hemispherical variation of the IRI's foF2 estimates at ±40° dip angle around 95°E and 130°E sector under fluctuating solar flux conditions

B.R. Kalita [a,b,*], P.K. Bhuyan [b], P. Nath [b], A. Hazarika [b], K. Wang [c]

[a] Department of Physics, Dibrugarh University, Dibrugarh 786004, India
[b] Centre for Atmospheric Studies, Dibrugarh University, Dibrugarh 786004, India
[c] Space Weather Services, Bureau of Meteorology, PO Box 1386, Level 15, 300 Elizabeth Street Surry Hills, New South Wales 2010, Australia

Received 15 May 2018; received in revised form 9 December 2018; accepted 10 December 2018
Available online 17 December 2018

Abstract

The deviation of the IRI estimates of the monthly mean foF2 in the low mid latitude of 95°E–130°E longitude sector is investigated using simultaneous ground measurements at four stations during 2010–2014. The stations form two conjugate pairs of the same geomagnetic latitude at two fixed longitudes enabling direct longitudinal and hemispheric comparison. The temporal, spatial, seasonal and solar activity variations of the deviations are discussed with reference to the longitudinal density variation in the transition region between low and midlatitudes. Cases of underestimation/overestimation as well as good estimate are noted. Underestimation (overestimation) in the daytime and overestimation (underestimation) in the nighttime of 95°E (130°E) are common. The longitudinal difference in the measurements suggests negative (positive) foF2 gradient from west to east in daytime (nighttime). In contrast, the IRI predicts flatter or increasing longitudinal profiles from 95°E to 130°E. The local time and longitudinal variation of the IRI deviations can be attributed to the combined role of the longitudinal EIA structure as well as midlatitude zonal wind-magnetic declination effect. The station/season independent deviations relate the role of solar activity representation in the IRI. These deviations may be attributed to the weak IRI response to rapid solar flux fluctuations.

Keywords: IRI; foF2; Longitudinal; EIA; Solar activity

1. Introduction

The longitudinal variation of the ionospheric properties in low and mid-latitude has attracted the attention of the ionospheric community in the last two decades. The longitudinal variation adds to the complex ionospheric variability of the low latitude region. Deminova (1993, 1995) reported a wavelike longitudinal structure in the critical frequency of the F2 layer along the equatorial region from the Intercosmos II satellite data. Sagawa et al. (2005) reported wavelike structure in the development of equatorial ionization anomaly (EIA) during March-June of 2002, at nighttime by analysing the OI 135.6-nm nightglow from Far Ultraviolet (FUV) Imager on board the IMAGE satellites, and, thereby, suggested a longitudinal structure with Wave Number Four (WN4) or 90° periodicity. Subsequently, longitudinal structures have been found in equatorial/low latitude Total Electron Content (TEC), density, EEJ, vertical drift, bottom-side thickness and in neutral parameters like O/N2, temperature, nitric oxide etc. (England et al., 2006, Kil et al., 2007, Scherliess et al.,

* Corresponding author.
E-mail address: bitapkalita@dibru.ac.in (B.R. Kalita).

https://doi.org/10.1016/j.asr.2018.12.011
0273-1177/

2008; Oberheide and Forbes, 2008; Liu et al., 2010; He et al., 2010). The peaks of the wave structure in equinox and June solstice are observed along the 100°E, 190°E, 270°E and 10°E in the midday period but move eastward and, are shifted by about 20°–30° in the nighttime (Lin et al., 2007; Kalita et al., 2015). In addition to seasonal, local time and solar activity variation (Liu and Watanabe, 2008), hemispherical asymmetry in the longitudinal structures is also reported (McDonald et al., 2008). The non-migrating diurnal tides are considered to be the source of the EIA longitudinal structure (Immel et al., 2006). In contrast, the longitudinal density variation in mid-latitude (Zhang et al., 2011, 2012; Zhao et al., 2013; Yu et al., 2016) is attributed to the effect of zonal wind climatology associated with the varying magnetic declination (Challinor and Ecceles, 1971). The eastward zonal wind produces upward (downward) drag in the region of positive (negative) or eastward declination angle leading to ascent (descent) of the F layer and subsequent enhancement (reduction) in density/TEC in the northern hemisphere. The effects are in the opposite direction for the same declination in the southern hemisphere.

The longitudinal variation introduces an additional forcing mechanism for incorporation in the ionospheric models which generally are less successful in the low latitudes as compared to the mid latitude. The International Reference Ionosphere (IRI) which is the standard empirical model for the ionosphere, replicates the longitudinal structure observed by CHAMP satellite reasonably well (McNamara et al., 2010) with Comite Consultatif International des Radio communications model (CCIR option) during the nighttime (2000LT). In low latitudes, the model sometimes underestimates and sometimes overestimates depending on solar activity and longitude, etc. (Luhr and Xiong, 2010; Bhuyan and Hazarika, 2013; Kakoti et al., 2017 etc.). The overestimation is attributed to the overestimation of the equatorial plasma fountain via the vertical drift in solar minimum whereas underestimation is attributed to the longitudinal structure as well as solar activity effects. Recent comparison of the IRI 2012 model with the low latitude NmF2 (Maximum density of F2 layer) as well as TEC measurements from 95°E (Bhuyan and Hazarika, 2013; Hazarika and Bhuyan, 2014; Kalita and Bhuyan, 2017; Kakoti et al., 2017) have revealed systematic differences in the 95°E sector which happens to be within the strongest WN4 peak. As most of these studies involved single station data, a multi-station investigation spanning a wider longitude region is required to ascertain the effect of the F region longitudinal variation in the IRI predictions. In the transition region from low to mid-latitudes where the F region may be affected by both the longitudinal variation of the EIA and the magnetic declination effect, the assessment of the model's performance is even more critical.

In this work, we have investigated the longitudinal structure of the IRI 2016 (Bilitza et al., 2017) in the India-East Asia-Northern Australia region using the simultaneous ionosonde measurements of F2 layer critical frequency foF2 at multiple *low* mid-latitude stations at two fixed geo-magnetic latitudes (~±40° dip). We examine the effect of temporal, longitudinal and solar activity variation on the monthly IRI estimates.

2. Data and methodology

The foF2 recorded by ionosondes at low latitude stations Dibrugarh (27.48°N, 94.8°E, 42° dip), and Okinawa (26.21°N, 127.68°E, 39° dip) in the northern hemisphere and Cocos Islands (12.2°S, 96.8°E, 42° dip) and Darwin (12.45°S, 130.95°E, 37° dip) in the southern hemisphere during geo-magnetically quiet periods ($Kp < 3$) of 2010–2014 are used for comparison with the IRI 2016 model. The locations of the stations are shown in Fig. 1. Dibrugarh and Okinawa (nearly same magnetic latitude) are at the outer slope of the northern EIA separated by about 35° in longitude. Cocos Islands and Darwin are magnetically conjugate to Dibrugarh and Okinawa respectively. Previous studies (Kalita et al., 2015; Kakoti et al., 2018) indicate that these stations with finite dip angle are in the transition region from low to midlatitudes.

The IRI 2016 model is run with the CCIR options for the F2 layer critical frequency. The variance between the observed hourly averaged foF2 and the IRI foF2 is investigated for the period of 2010–2014. The differences are considered significant when it is higher than the standard deviation of the data. The monthly mean of F10.7 in sfu ($1sfu = 10^{-22}\,W\,m^{-2}\,Hz^{-1}$) is used as indicator of solar activity. SAMI2 Another Model of the Ionosphere (Huba et al., 2000) model is used to assess the effect of vertical drift on the low latitude foF2. The SAMI2 is an open source theoretical model which calculates the evolution of the low- to mid-latitude ionosphere in terms of seven ion species (H^+, He^+, N^+, O^+, $N2^+$, NO^+, and O^{2+}) in the altitude range 85–20,000 km through the dynamic and chemical properties of the plasma. The continuity and momentum equations are solved for all 7 species; the temperature equation is solved for H^+, He^+, O^+, and the electrons. The plasma along the earth's geomagnetic field from hemisphere to hemisphere is modelled using an offset, tilted dipole field. The ExB drift of the plasma and the parameters of the neutral species can be modelled by the user. The parameter NmF2 (the maximum density of the F2 layer) is obtained from SAMI2 vertical density profile and is related to critical frequency of F2 layer foF2 by the following relation-$NmF2 = 1.24 \times (foF2)^2 \times 10^{10}$ in per m^3 where foF2 is in MHz.

3. Results

3.1. The comparison of the quiet time monthly mean foF2 with the IRI

Kalita and Bhuyan (2017) compared the seasonal variation of the F region parameters measured with a Canadian Advanced Digital Ionosonde (CADI) over Dibrugarh with those of the IRI 2012 and found underestimation by the

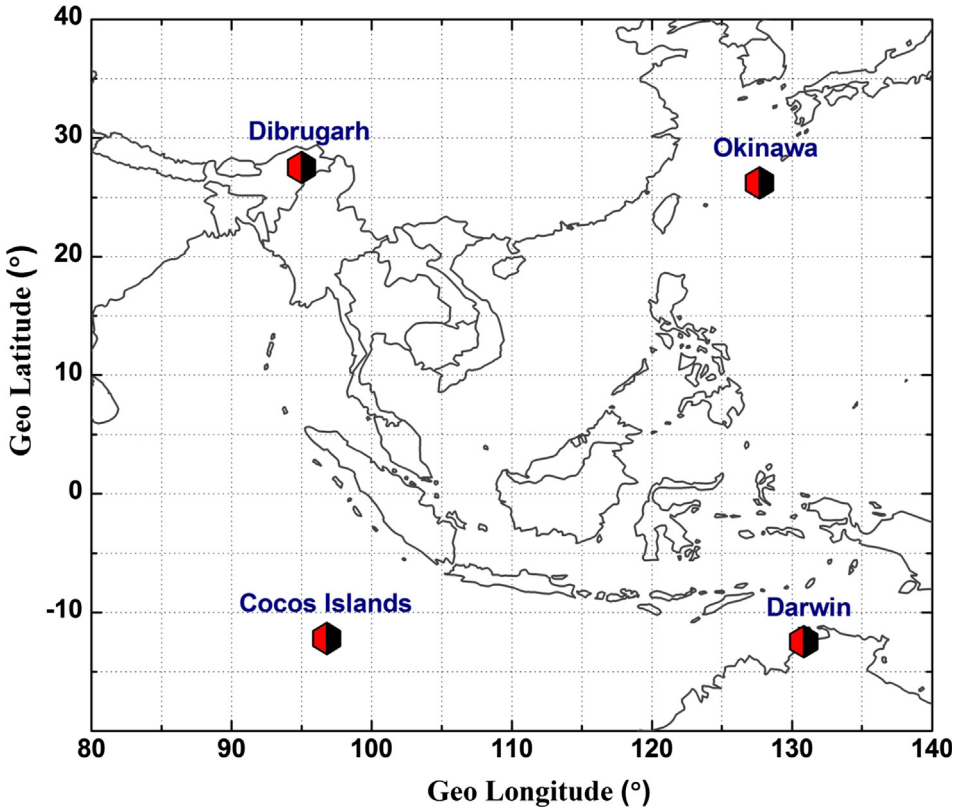

Fig. 1. The map of the observatory/stations used in this study.

model in March equinox. Figs. 2 and 3 shows the diurnal variation of the ΔfoF2 (monthly mean $foF2_{Obs}$-$foF2_{IRI}$) over the northern and southern hemisphere stations (details in section 2 above) for low (from August 2010 to August 2011) and high (from September 2011 to July 2014) solar activity conditions respectively, during the ascending phase of the current solar cycle 24. The monthly mean $F10.7 < 100$ is considered as low and $F10.7 \geq 120$ is considered high solar activity. The positive (negative) values of ΔfoF2 indicate underestimation (overestimation) by the IRI model. It is evident that the difference between the observed values and the model predictions varies with local time, month, season, solar activity and observing location. In the southern hemisphere (SH), during the low solar activity period the model underestimates the foF2 during the equinoctial months of March-April and overestimates the foF2 during July-August in the post noon period. The trend over Darwin is mostly of overestimation whereas the trend over Cocos Islands (CI) in the daytime is that of either agreement or underestimation whereas in the nighttime it is of overestimation. In the northern hemisphere, during the low solar activity period, the IRI 2016 estimates differ significantly from the observed foF2 over Dibrugarh during midday of March-April. The ΔfoF2 fluctuates with local time between positive and negative from September to February but it remains positive throughout the day in March-April. Good agreement is seen in May-June. In contrast, over Okinawa, the IRI tends to overestimate (except March-April) the daytime foF2 but underestimate the nighttime values, particularly in the equinoctial months. Between the hemispheres, the IRI mostly overestimates (agrees) in the respective winter (summer). In most months the diurnal trend of ΔfoF2 varies with local time and the same (different) meridian stations are in phase (out of phase). In general, in this low activity period till August 2011, the largest (smallest) difference between the measured foF2 and the model values are noted in the equinoctial period (solstice months of May-July) but there is significant local time, longitudinal and hemispheric asymmetry in the ΔfoF2.

The solar activity increases in September 2011 and fluctuates between 100 and 170 sfu (F10.7) till July 2014. In this period the months with mean $F10.7 \geq 120$ are considered as high solar flux condition. In the southern hemisphere (Fig. 3), the IRI estimates agree with the foF2 over Darwin from September to December and in the forenoon period of January to April months. Post noon underestimation from January to April reverses to whole day overestimation from May to August (winter). The limited data from Cocos Islands in high solar flux indicate underestimation during the equinoctial months and overestimation during May-June. In general, the IRI estimates are better in the early morning to midday period as compared to the nighttime. In the northern hemisphere (Fig. 3), the ΔfoF2 over Dibrugarh fluctuates from September-

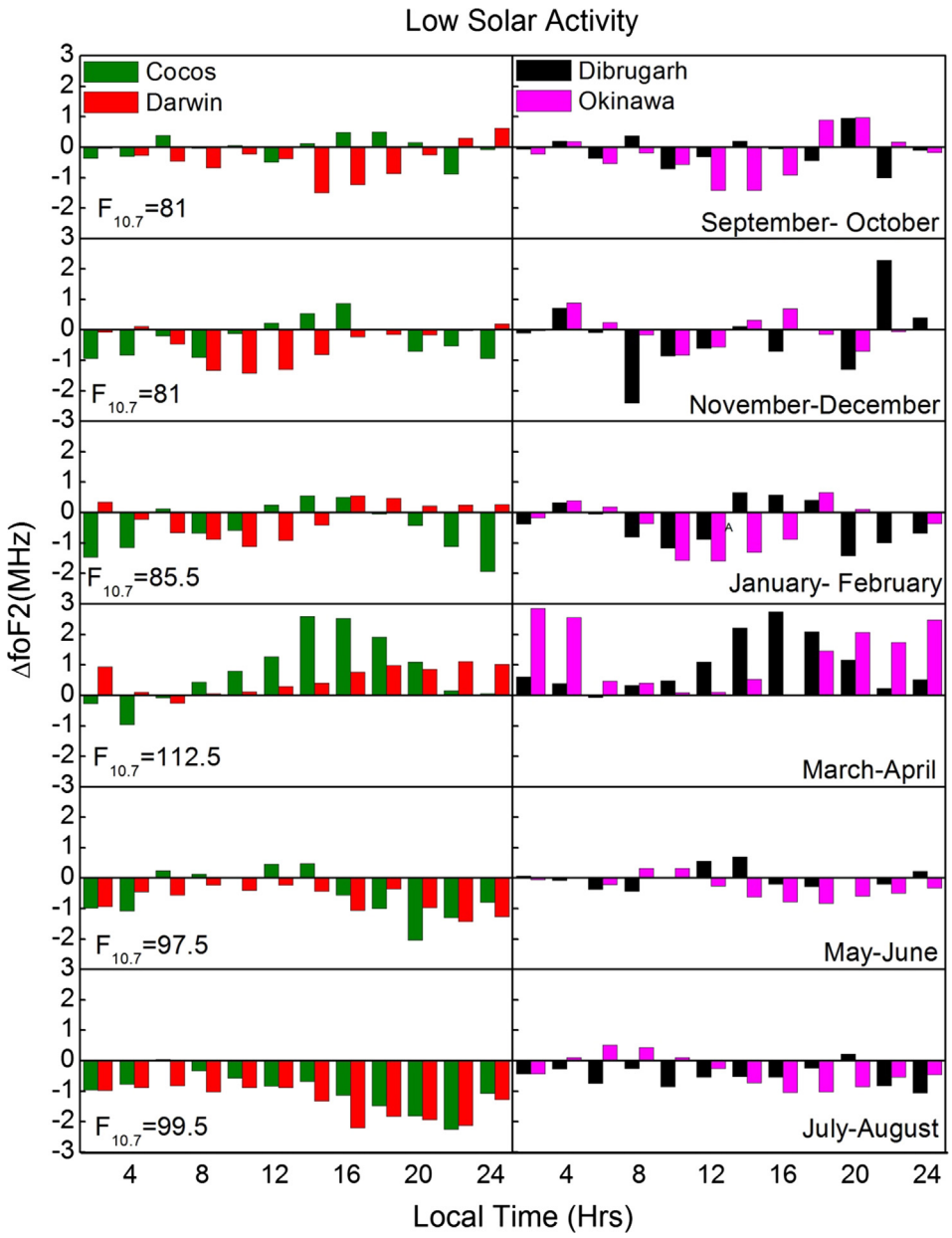

Fig. 2. The longitudinal variation of ΔfoF2 ($foF2_{Obs}$-$foF2_{IRI}$) at southern (left) and northern hemisphere (right) low mid-latitude stations (±40° dip) for the low solar activity period of August 2010 to August 2011. Dibrugarh –Cocos Islands at 95°E and Okinawa-Darwin at 130°E form conjugate pairs.

October (positive in afternoon) to November-December (negative in nighttime).

During January-February, the positive trend in the daytime reverses to negative in the nighttime. The IRI underestimates the Dibrugarh foF2 during March-April (post noon) and July-August but agrees fairly well in May-June period. The ΔfoF2 over Okinawa is predominantly negative except during the nighttime of equinox months and afternoon period of July-August. Good agreements are seen during May-June (northern summer) and midday of March-April. The trend as well as the phase is similar to that over Dibrugarh during March -April and July-August, but a phase difference is noted in other months. Between the hemispheres, agreement during the respective summer solstice and overestimation during the winter solstice is noteworthy. In this period of high solar flux, the observed difference with the IRI increases.

Therefore, the IRI generally underestimates in March equinox, overestimates in winter and agrees with observation in summer. The hemispherical differences are prominent only during the solstice and seem to be related to the seasonal changes. The local time variation shows that the ΔfoF2 in the same meridian (conjugate stations) is mostly in phase. But, longitudinally, the two sectors are mostly out of phase in the northern hemisphere with the changes in 130°E lagging by about 6–8 h (Figs. 2 and 3). Daytime underestimation (overestimation) at Dibrugarh (Okinawa) is common. In the southern hemisphere, the

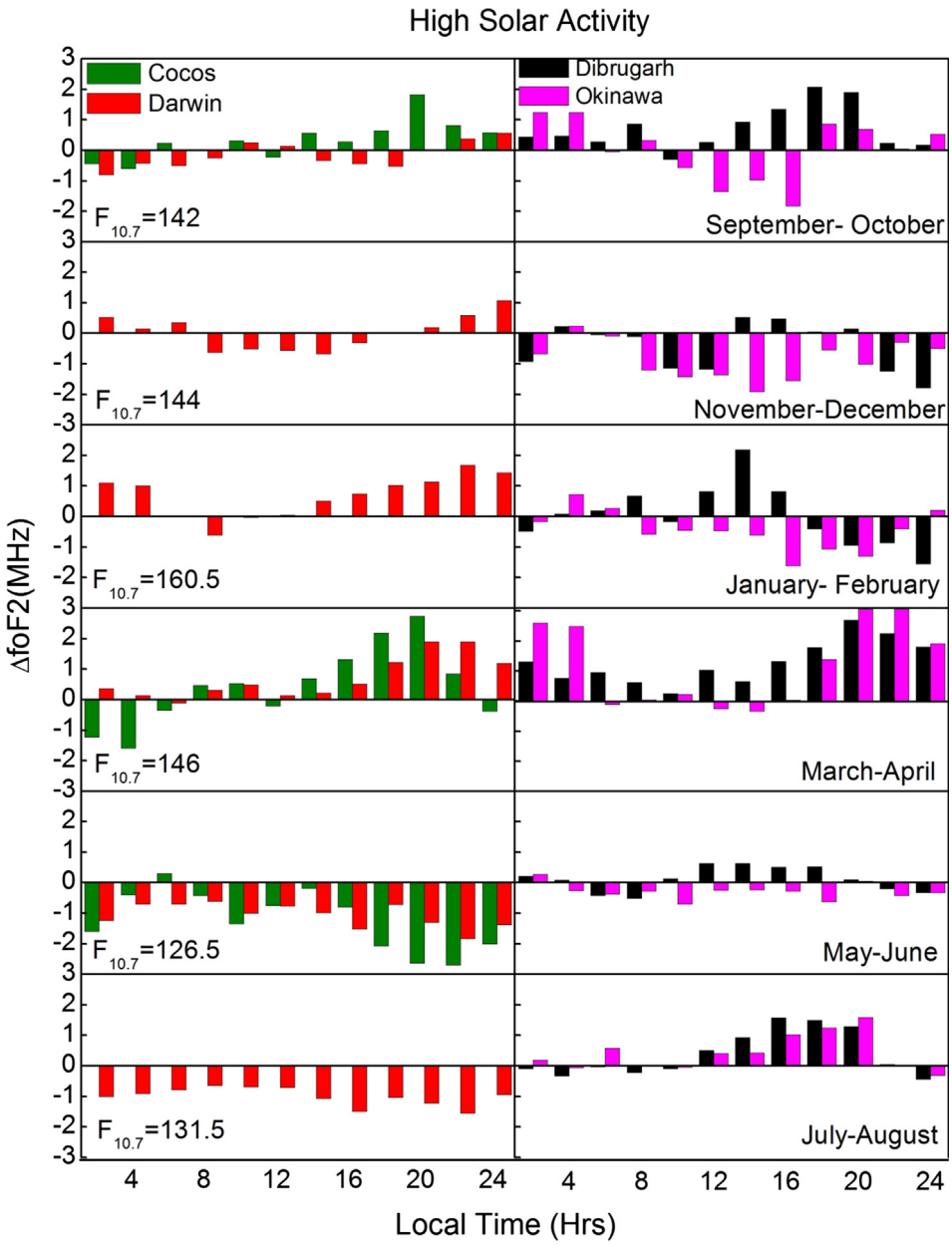

Fig. 3. Same as Fig. 2 for the high solar activity period (September 2011-August 2014). Only data for F10.7 > 120 is used.

two longitudes show both in phase and out of phase relation with mostly underestimation in Cocos Islands and overestimation in Darwin. The monthly and seasonal trend is obscured by the solar activity variation. Quantitatively, the minimum (maximum) variance between the measured values and the model estimates are observed during the summer solstice (March equinox). In terms of local time, the maximum (>2 MHz) difference over Dibrugarh, Cocos Islands and Darwin is noted in the afternoon to post sunset hours (Figs. 2 and 3) and the minimum difference is observed during late night-early morning hours (<0.1 MHz). In contrast, the difference between the measured foF2 over Okinawa/Darwin and the IRI estimate is maximum (>3.5 MHz) during the evening to nighttime and minimum (<0.1 MHz) during the forenoon hours (Fig. 3).

4. Discussion

In this study, while examining the performance of the global IRI we haven't considered the possible contribution of the insufficient data input into the IRI from the 95°E longitude although only interpolations may have been used in the current IRI for this region.

In addition to the lack of sufficient input from the 95°E sector to the IRI, there are multiple variables affecting the daily variation of the difference between the observed mean foF2 and the IRI estimates presented in results section-(1)

latitude and longitude of observation (2) local time and month (3) solar activity and (4) finally the IRI representation of these factors. We discuss below how these factors affect the foF2 and how the IRI attempt to reproduce these forcing.

4.1. IRI performance vis a vis longitudinal and hemispherical variations

Firstly, we focus on the longitudinal and hemispherical variation of the IRI performance which is also linked to the local time and seasonal variation respectively. The geographic region under consideration in this study mainly encompasses north-east India, south-east Asia and northern Australian region at two specific latitudes (~27°N and ~12.5°S) and longitudes (~95°E and ~130°E). The trends are qualitatively similar in the same longitudes but opposite in the two longitudes under study, with subtle differences between the hemispheres. To examine this longitudinal asymmetry, the longitudinal foF2 profiles predicted by the IRI for the month of April (2012), June (2013) and December (2013) during 1400LT and 2000LT for 27° N and 12.5°S are shown in Fig. 4. It is evident from the figure that the IRI doesn't reproduce a notable longitudinal structure in the northern low latitudes except during daytime winter conditions (December). In contrast, longitudinal variation is predicted in the southern low latitudes except during daytime of summer (December). The IRI predicts higher foF2 in the 120°–130°E sector as compared to the 95°E sector in all conditions except during daytime of northern winter and nighttime of northern summer. Previous observational studies (Kalita et al., 2015) suggest that foF2/NmF2 in Dibrugarh-Okinawa latitude is higher (lower) in the 95°E sector as compared to the 130°E sector in the daytime (nighttime). To investigate the longitudinal foF2 variation in the southern latitudes, the local time variation of the difference between the monthly mean measured foF2 over Cocos Islands and Darwin are shown in Fig. 5 for the sample year 2011. The observed foF2 in the 95°E is lower than that in the 130°E sector only during the post midnight and early morning period but higher during the rest of the day. Therefore, observations suggest a negative (flat or positive) longitudinal gradient similar to that in the northern hemisphere from 95°E to 130°E during the post noon period (nighttime) whereas the IRI uses a positive gradient, which leads to the systematic difference between the observed foF2 and the model estimates. In the southern hemisphere, the IRI overestimates in the 130°E sector because the model consistently predicts a peak around 120°E longitudes. The local time variation ΔfoF2 characterised by the distinctive reversal of daytime underestimation (overestimation) to nighttime overestimation (underestimation) in 95°E (130°E) as well as the west-east difference clearly indicates an evolving longitudinal structure. Previously, Lin et al. (2007) have shown that the four peaked EIA longitudinal structure evolve with local time and tend to move eastward with a velocity of several tens of meters per second. In particular, the daytime density

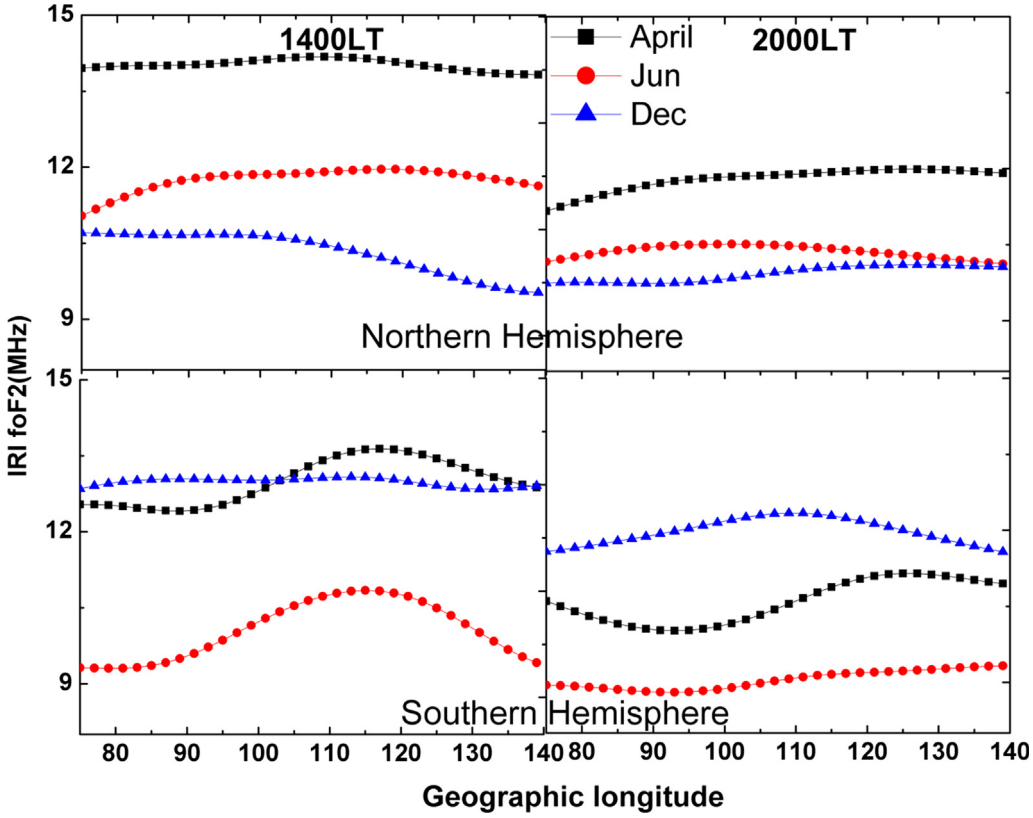

Fig. 4. The IRI foF2 longitudinal profiles for the northern hemisphere at 27°N and the southern hemisphere at 12.5°S.

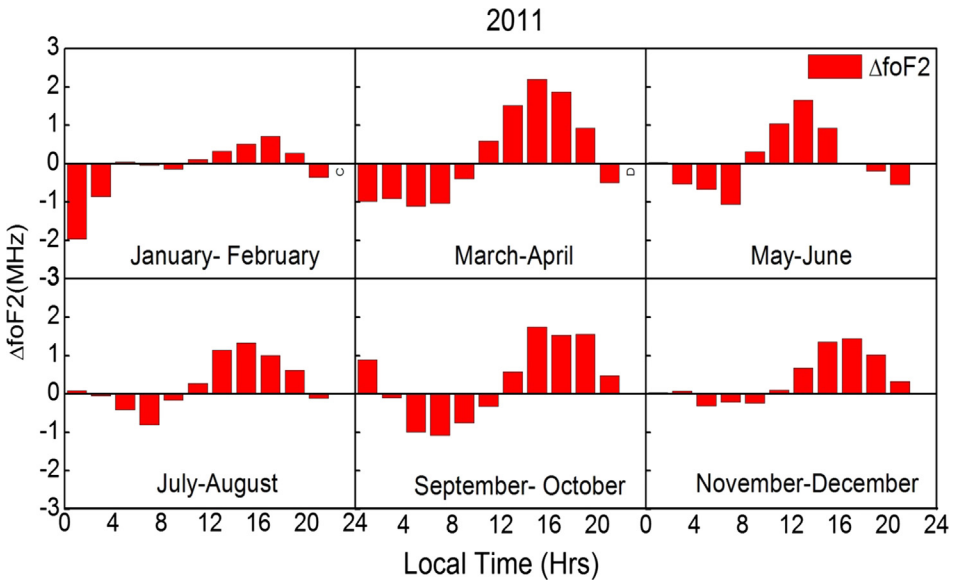

Fig. 5. The local time variation of the ΔfoF2 ($foF2_{Cocos\ Islands}$-$foF2_{Darwin}$) showing the east-west difference in the southern hemisphere.

peak along 90°–100°E moves to around 120°E by nighttime (Liu and Watanabe, 2008). Previous studies (Kalita et al., 2015; Kakoti et al., 2018) using both NmF2 and TEC data from this region suggest that the stations Dibrugarh, Okinawa and Cocos Islands are affected by the EIA, but the effect varies with season and solar activity. The latitudinal foF2 profile of IRI 2016 (not shown) predictions place these stations inside the anomaly region.

The strength of the EIA/plasma fountain is controlled by the equatorial vertical drift (E × B) and the drift estimated from the ROCSAT-1 measurements (Kil et al., 2007, 2008) indicates clear longitudinal variation with daytime (nighttime) peak near 90°–100°E (120°E). Therefore, the evolving longitudinal EIA structure can manifest as daytime (nighttime) underestimation in the western (eastern) sector.

We note that the magnetic dip angles at the four stations are around 37°–42° (section 2), and, therefore, significant effects of neutral winds cannot be ruled out. Kalita et al. (2015) have shown that Dibrugarh can behave like a midlatitude station particularly during the December solstice. The longitudinal density variation in the midlatitude exhibits day-night structure due to the changing direction of the zonal winds from westward in the daytime to eastward in the nighttime (Zhang et al., 2011, 2012 etc.). The mechanism for longitudinal variation in midlatitude depends on the east–west difference in magnetic declination as illustrated in Fig. 5 of He et al. (2011) and Fig. 2 of Zhang et al. (2012). In the longitude range under consideration, the magnetic declinations are less (as compared to the American sector) but finite, and, can lead to an east-west density difference (Zhao et al., 2013; Yu et al., 2016). The magnetic declinations for the four stations used in this study are shown in the Table 1.

Therefore, an east-west difference of around 5° in declination can be assumed for the station pairs. In the northern hemisphere, the declination effects should be negligible over Dibrugarh whereas it should contribute finitely over Okinawa. In the southern hemisphere, the classic positive and negative declination at Darwin and Cocos Islands respectively with zero declination in between creates the right configuration for the westward (eastward) zonal wind in daytime (nighttime) to produce a downward (upward) drag in the 130°E sector (Zhang et al., 2012 etc.). Consequently, the daytime density in this sector would be reduced and nighttime density would be enhanced. The opposite effect due to negative declination may lead to enhancement in the daytime over Cocos Islands and consequently to the underestimation effect. The seasonal and hemispherical variation of the zonal wind together with the hemispherical asymmetry in the field line geometry may lead to the slightly different temporal variation of the trend in the northern and southern hemisphere. Here we are not considering the effect of the meridional wind as longitudinal variation of the meridional wind at such longitude scale is not reported.

Table 1
The magnetic declination at the northern and southern stations from the IGRF model.

Dibrugarh (27.48°N, 94.8E°)	Okinawa (26.21°N, 127.68°E)
Declination ~0.48°W	Declination- ~5.3°W
Cocos Islands (12.2°S, 96.8°E)	Darwin (12.46°S, 130.84°E)
Declination ~2.3°W	Declination ~3°E

4.2. The role of longitudinal variation of E × B vertical drift and magnetic declination

To examine relative role of the equatorial vertical drift induced plasma transport and the magnetic declination effect, we simulate the NmF2 over Dibrugarh and Okinawa using the SAMI2 physical model, and, the results (after

conversion of NmF2 to foF2) are shown in Fig. 6 for March 2014 condition. The equinoctial month is chosen to eliminate the effect of the inter-hemispheric neutral winds. The observed and model values are shown in the top panel of Fig. 7 for Dibrugarh in 95°E and for Okinawa in 130°E sector. In the bottom panel the ROCSAT-1 empirical model (Kil et al., 2008) vertical drift along with the drift models used in the SAMI2 and IRI model are shown. In contrast to the IRI, which underestimated Dibrugarh foF2 from forenoon to pre-midnight, the SAMI2 foF2 is nearly the same as of that of Dibrugarh. The IRI shows very good agreement with daytime measurements over Okinawa but underestimates the post noon foF2. These results have been discussed previously with Fig. 3. The SAMI2 overestimates (underestimates) the daytime (post mid night) values over Okinawa. Interestingly, the vertical drift over Dibrugarh is higher according to the empirical model, which may lead to stronger fountain effect and the resultant daytime underestimation in the equinoctial months. The similarity in the empirical model drift and the IRI drift in the 130°E sector corresponds to the good agreement between the IRI and the observation at Okinawa during daytime. We run the SAMI2 over Okinawa again by reducing the drifts to compensate for the overestimation over Okinawa. The simulated density with reduced (half) vertical drift matches the observed values

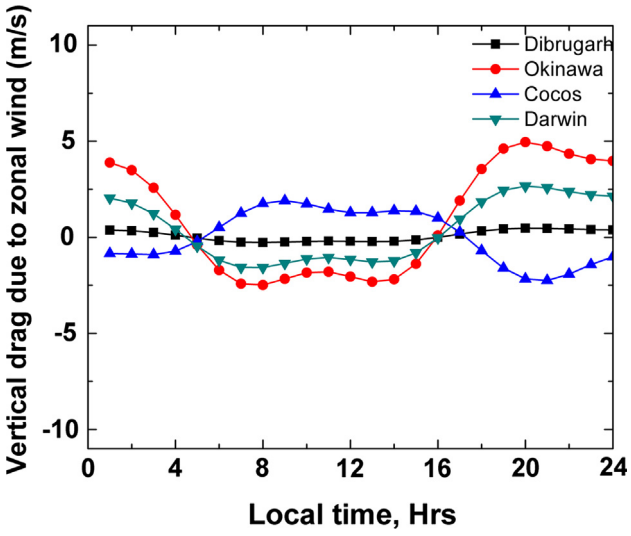

Fig. 7. The vertical drag for March 2014 induced by the zonal wind due to the finite magnetic declination. The positive values are for upward drag. Nighttime upward drag in the 130°E sector can be noted.

in daytime, but it is lower than the observed density in the nighttime. Therefore, the equatorial vertical drift and consequently the EIA may play a role in the daytime density variation over this low midlatitude region, but other factors may also be effective, particularly in the nighttime

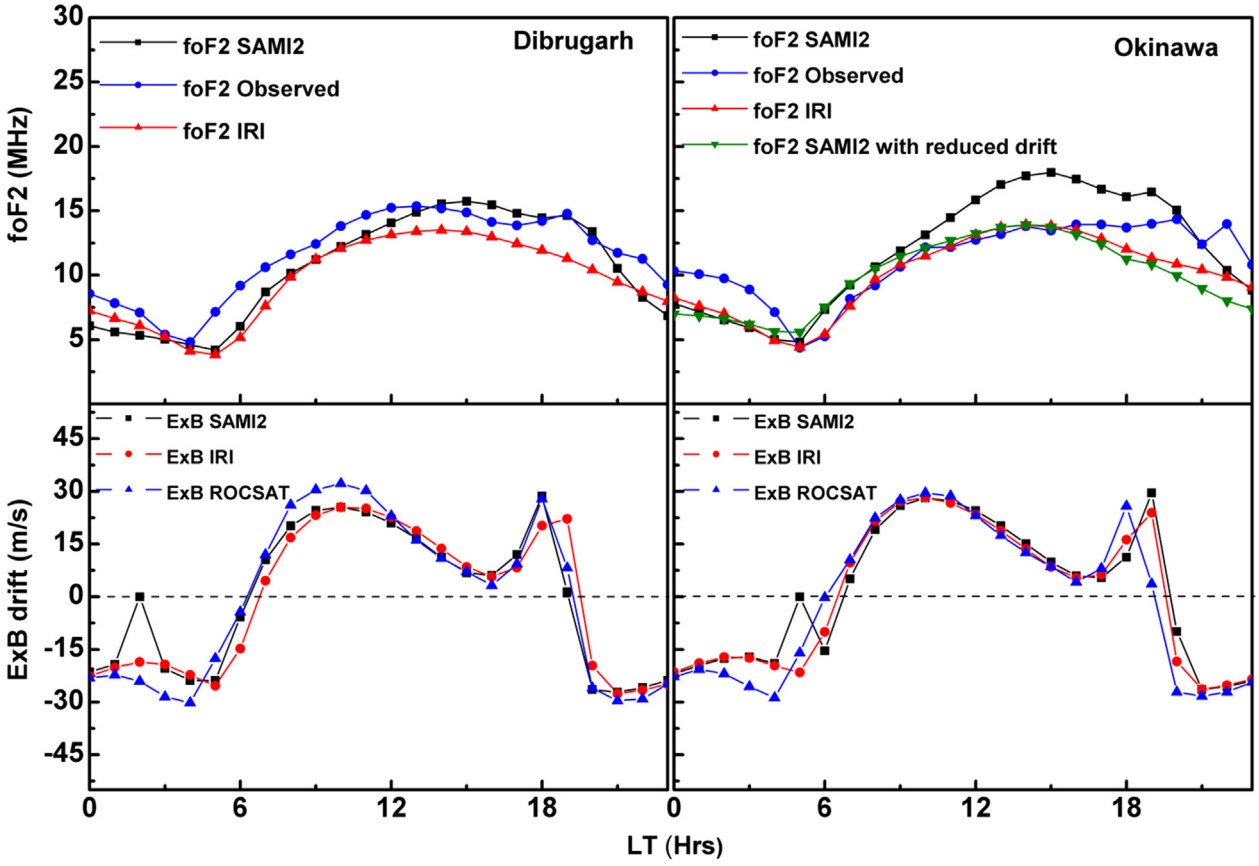

Fig. 6. The observed and model foF2 at Dibrugarh and Okinawa and the respective E × B drift for March 2014. Note the role of the E × B drift in the IRI performance in the two sectors.

as empirical model vertical drift estimates seems quite reliable. Increase of winds in the SAMI2 model reduces the nighttime density (not shown) without affecting the daytime density (foF2). To examine the effect of the zonal wind due to the finite magnetic declination, we calculate the vertical drag as given by U_{zon} SinDCosISinI, where U_{zon} is the zonal wind from the HWM14 wind, D is declination angle and I is the inclination angle at the respective stations. The effective vertical drifts (Titheridge, 1995) at the four stations are shown in Fig. 7. A westward (eastward) zonal wind in the daytime (nighttime) would produce a downward (upward) drag at Okinawa/Darwin. The upward drag in the nighttime leading to the higher altitude of the F layer helps sustain the density due to lower recombination at higher altitude. Previous studies of hmF2 variation (Kalita et al., 2015) indicate higher altitude of the nighttime F2 layer over Okinawa as compared to that over Dibrugarh. The nearly 5 m/s difference in the nighttime vertical drag leading to F layer height difference between the two longitudes may partially account for the higher nighttime density in the eastern longitude and the consequent underestimation by the IRI.

4.3. The role of solar activity in the measured and the model foF2

Now, we discuss the role of solar activity in the ΔfoF2 variations. We have noted that the deviations of the IRI in certain months are one directional in all the stations. Rapid fluctuations in the solar activity prior to these periods seem to be related to the uncharacteristic IRI behaviour, where the regular seasonal pattern of ΔfoF2 (noted in section 3 from Figs. 2 and 3) are missing. The IRI representation of the solar activity effect of the ionospheric density particularly NmF2 (foF2)/TEC have been subjected to numerous scrutiny, and, certain deviations from the observed solar activity trend were noted, particularly on the solar activity variation of daily values (Kakoti et al., 2017 and references therein). In this study, we have noted the diverse response of the monthly mean ΔfoF2 to solar forcing, and, we attempt to ascertain the underlying conditions.

A time line of the IRI response with solar activity variation is presented in Fig. 8 in form of monthly ΔfoF2 to show the response of the model to the stimulus of rapid

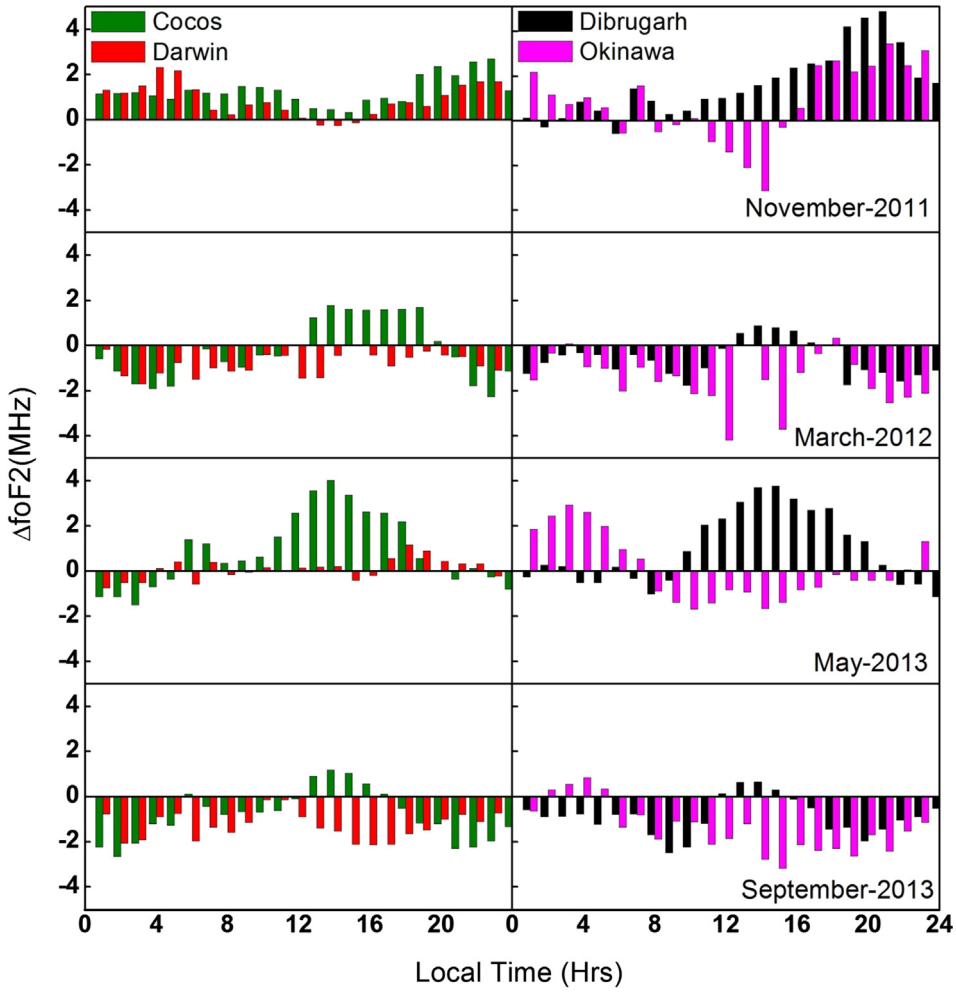

Fig. 8. The ΔfoF2 ($foF2_{Obs}$-$foF2_{IRI}$) for periods of rapid solar flux variation. The ΔfoF2 trend is different from the seasonal trend observed in Figs. 2 and 3.

solar activity fluctuations. The IRI usually overestimates (agrees with) the nighttime foF2 in the month of November-December (second panel Figs. 2 and 3) for northern winter (southern summer), but, when solar activity increases rapidly from 103 sfu (monthly F10.7) in August 2011 to about 149 sfu in November 2011, we note that the IRI underestimates the measured foF2, particularly over Dibrugarh by more than 5 MHz in the post sunset period (top right panel Fig. 8). This is followed by reasonably good agreement or overestimation in March 2012, whereas the IRI generally underestimates the foF2 in March equinox (Figs. 2 and 3). To illustrate this point, we have compared the daily variations of foF2 over Dibrugarh and Cocos Islands in March 2011 and March 2012 with their respective IRI estimates in Fig. 9. The solar activity in March of 2011 and 2012 are similar (F10.7–115) and the means of the measured foF2 are also similar with peak around 14–15 MHz but the IRI estimates are different. The model predicts higher foF2 (>2 MHz) in March 2012 as compared to 2011 in the afternoon to the pre-midnight period. The IRI estimates higher (lower) values for March 2012 (November 2011) as compared to March 2011 probably because the solar activity in the preceding time period of March 2012 (November 2011), i.e. November-December 2011 (July-August 2011) is higher (lower). The IRI uses the twelve months running mean ionospheric index IG_{12} with the CCIR (1967) foF2 model (Bilitza et al., 2017) which is closely correlated ($R \sim 0.98$) with the 12-month running mean of sunspot number (Rz_{12}). The IG_{12} (Rz_{12}) is around 79 (66) in March 2012 as compared to 31 (35) in March 2011. Therefore, the IRI estimates higher and better in March 2012 when the solar activity is increasing steadily but couldn't reproduce the post sunset foF2 increase in November 2011 when the solar activity jumps in the previous months. The IRI uses a semi-annual foF2 variation with equinoctial peaks, and, the lower estimates in November 2011 could partly be due to the seasonal dependence of the IRI solar activity trend. Interestingly, the IRI underestimates the foF2 in the 95°E sector in May 2013 (Fig. 8) as F10.7 increases, and, subsequently overestimates the foF2 in September 2013 as the solar activity decreases sharply. This is a break away from the regular trend of good agreement (overestimation) of the IRI with observations in May-June period for northern (southern) hemisphere and underestimation/agreement in September-October period (Figs. 2 and 3). To illustrate the relation of the IRI deviation with solar activity, we show the daytime integrated monthly mean foF2 over Dibrugarh and Cocos Islands with the monthly mean F10.7 and IG_{12} for the period of August 2010 to June 2014 in Fig. 10. Daytime integration or sum over all hours is used to eliminate the local time bias. A pattern of alternate underestimation during increasing phase/high of solar activity and overestimation during decreasing phase/low of solar activity is evident. Overestimation in low solar flux and underestimation in high solar flux by the IRI was also noted by Bhuyan and Chamua (2002) for topside measurements over Indian zone. From Fig. 10, we note that the IG_{12} variation after September 2011 is slow and minimal. The highest IRI peak is noted March-April 2012 corresponding to the flat peak in IG_{12}, delayed from the November 2011 peak in F10.7. The second peak of IG_{12} is noted around August 2014 whereas the F10.7 peaks in February 2014. The measured foF2 pattern over Dibrugarh and Cocos seems to follow the monthly variation of the F10.7 (except for the seasonal bias during June solstice) whereas the IRI foF2 clearly follows the IG_{12}. Therefore, during the rapid solar flux variation in the time scale of 3–4 months, the twelve months averaging IG_{12} would introduce higher (lower) input to the model at the down-swing (up-swing)

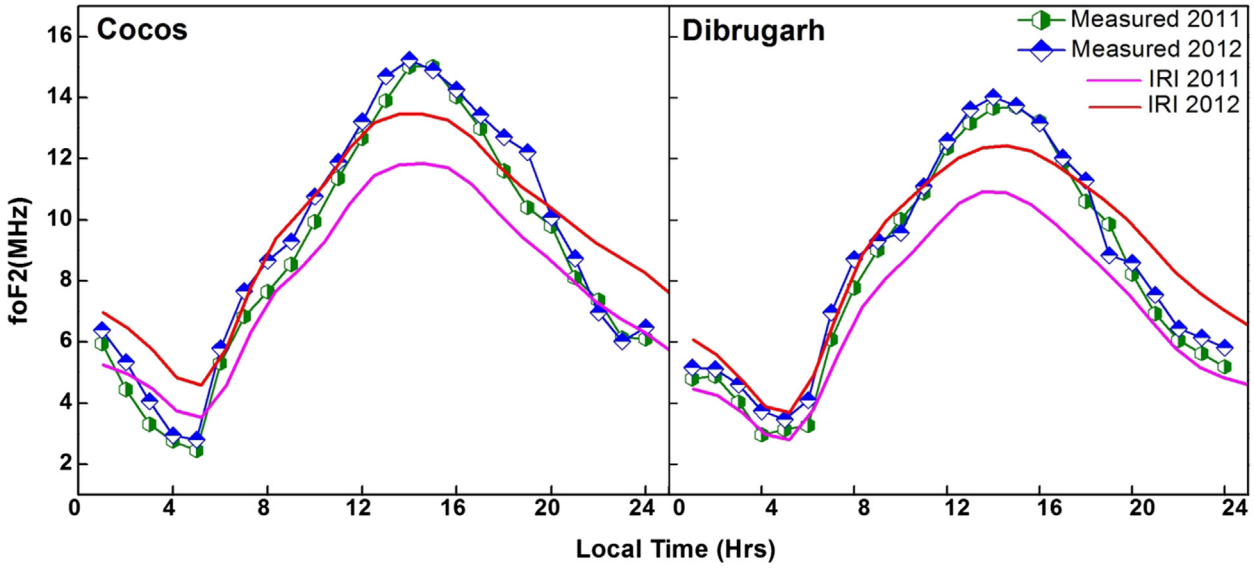

Fig. 9. The variation of the foF2 and the IRI estimates over Dibrugarh and Cocos Islands during March 2011 and March 2012. The measured values in these months are similar but the IRI predictions differ widely corresponding to similar F10.7 but different IG_{12}/Rz_{12}. respectively.

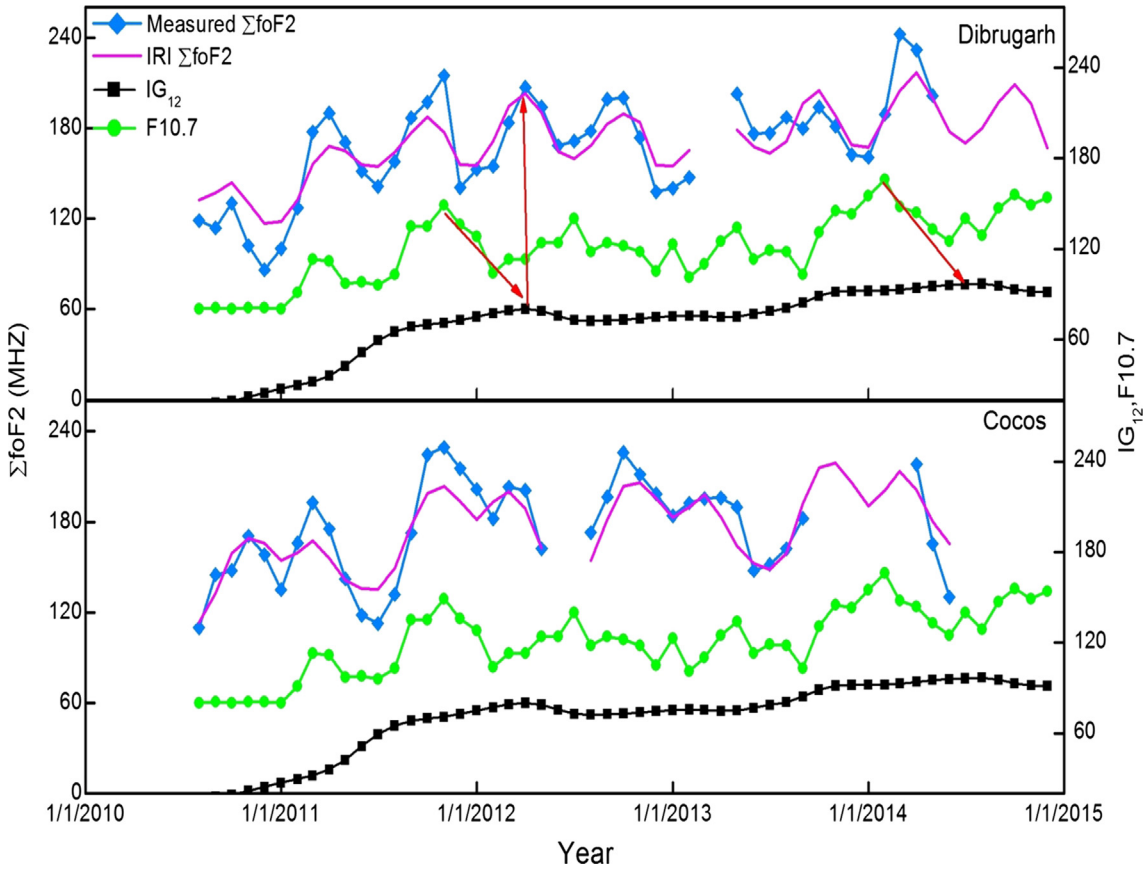

Fig. 10. The variations of the integrated (sum over all hours) foF2 over Dibrugarh and Cocos Islands with monthly mean F10.7 and IG_{12}. Underestimation during high solar flux and overestimation during low solar flux can be noted. The delayed peak in IG_{12} as compared to F10.7 and the corresponding IRI estimate is shown by the arrows.

producing higher (lower) estimates. We also note that the IRI as well as observation responds differently to solar flux variation in equinox and solstice e.g. July 2012, November-December 2013 and March 2014. This seasonal dependence of the solar activity effect conceals the true solar activity response. In general, the IRI responds weakly to the rapid changes in solar activity probably due to the slow temporal variation of the IG_{12} index. The solar activity response is easily perceptible only in the 95°E sector probably due to the lack of data input to the IRI from this region.

5. Summary and conclusions

The difference between the observed monthly mean foF2 and the IRI foF2 is examined for the period of 2010–2014 in two magnetically conjugate low mid-latitude station pairs in the 95°E and 130°E longitude sectors. The temporal, spatial, seasonal and solar activity variations of the IRI deviation from observation are discussed to assess the relative role of these factors on the IRI estimates. Cases of underestimation as well as overestimation are noted depending on observing station, local time, season and solar activity. Clear local time variation of the ΔfoF2 with phase lag between 95°E and 130°E are noted in most months. The IRI longitudinal profiles in both hemispheres show a flat or positive density gradient from west to east, whereas the observation indicates opposite foF2 gradient in the daytime. The month-to-month fluctuation of solar activity in the solar cycle 24 added to the complexity of the seasonal variation, and thereby led to IRI performance degradation. The IRI was found to react weakly to rapid fluctuations in solar activity leading to the underestimation during upswing and overestimation in the downswing. The main conclusion of the study can be summarized as follows-

1. The source of the underestimation/overestimation of the foF2 at the low to midlatitude transition region within India-east Asia-north Australia zone could be the longitudinal variation caused by the longitudinal variation in the EIA as well as the longitudinal variation in the magnetic declination.
2. The IRI's estimate of the monthly mean foF2 deviates from observations due to weak reaction of the model to rapid solar fluctuations.

Acknowledgements

The authors acknowledge the ISRO-SSPS program for funding the CADI ionosonde at Dibrugarh. P.K.B. would like to acknowledge the UGC for Emeritus Fellowship.

The authors would like to thank Hyosub Kil for the ROCSAT vertical drift model. The authors would like to thank Dr. J. Huba for using the SAMI2 model ionospheric which was written and developed in the Naval Research Laboratory. The authors also acknowledge the use of the HWM14 model for thermospheric winds.

References

Bhuyan, P.K., Chamua, M., 2002. Electron density measurements in the topside F-region and its comparison with the IRI in the 75°E longitude sector. J. Atmos. Terr. Phys 64 (1), 55–64. https://doi.org/10.1016/S1364-6826(01)00094-3, ISSN 1364-6826.

Bhuyan, P.K., Hazarika, R., 2013. GPS TEC near the crest of the EIA at 95°E during the ascending half of solar cycle 24 and comparison with IRI simulations. Adv. Space Res. 52, 1247–1260. https://doi.org/10.1016/j.asr.2013.06.029.

Bilitza, D., Altadill, D., Truhlik, V., Shubin, V., Galkin, I., Reinisch, B., Huang, X., 2017. International Reference Ionosphere 2016: from ionospheric climate to real-time weather predictions. Space Weather 15, 418–429. https://doi.org/10.1002/2016SW001593.

CCIR, 1967. Consultative Committee on International Radio, Atlas of Ionospheric Characteristics, Report 340. International Telecommunication Union, Geneva, Switzerland.

Challinor, R.A., Ecceles, D., 1971. Longitudinal variations of the mid-latitude ionosphere produced by neutral-air winds—I Neutral-air winds and ionospheric drifts in the northern and southern hemispheres. J. Atmos. Terr. Phys. 33, 363–369. https://doi.org/10.1016/0021-9169(71)90141-3.

Deminova, G.F., 1993. Wave-like structure of longitudinal variations in the nighttime equatorial ionosphere. Geomagn. Aeron. 33 (5), 167–169.

Deminova, G.F., 1995. Wave structure of longitudinal variations in the nighttime equatorial anomaly. Geomag. Aeron. 35 (4), 169–173.

England, S.L., Maus, S., Immel, T.J., Mende, S.B., 2006. Longitudinal variation of the E-region electric fields caused by atmospheric tides. GeoPhys. Res. Lett. 33, L21105. https://doi.org/10.1029/2006GL027465.

He, M., Liu, L., Wan, W., Lei, J., Zhao, B., 2010. Longitudinal modulation of the O/N_2column density retrieved from TIMED/GUVI measurement. GeoPhys. Res. Lett. 37, L20108. https://doi.org/10.1029/2010GL045105.

He, M., Liu, L., Wan, W., Zhao, B., 2011. A study on the nighttime midlatitude ionospheric trough. J. GeoPhys. Res. 116, A05315. https://doi.org/10.1029/2010JA016252.

Hazarika, R., Bhuyan, P.K., 2014. Spatial distribution of TEC across India in 2005: seasonal asymmetries and IRI predictions. Adv. Space Res. 54 (9), 1751–1767. https://doi.org/10.1016/j.asr.2014.07.011.

Huba, J.D., Joyce, G., Fedder, J.A., 2000. Sami2 is Another Model of the Ionosphere (SAMI2): a new low-latitude ionosphere model. J. GeoPhys. Res. 105, 23035–23053. https://doi.org/10.1029/2000JA000035.

Immel, T.J., Sagawa, E., England, S.L., Henderson, S.B., Hagan, M.E., Mende, S.B., Frey, H.U., Swenson, C.M., Paxton, L.J., 2006. The control of equatorial ionospheric morphology by atmospheric tides. GeoPhys. Res. Lett. 33, L15108. https://doi.org/10.1029/2006GL026161.

Kakoti, G., Bhuyan, P.K., Hazarika, R., 2017. Seasonal and solar cycle effects on TEC at 95°E in the ascending half (2009–2014) of the subdued solar cycle 24: consistent underestimation by IRI 2012. Adv. Space Res. 60, 257–275. https://doi.org/10.1016/j.asr.2016.09.002.

Kakoti, G., Kalita, B.R., Hazarika, R., Bhuyan, P.K., Sharma, S., Tiwari, R.C., 2018. Temporal evolution of the EIA along 95°E as obtained from GNSS TEC measurements and SAMI3 model. Adv. Space Res. 61, 2837–2853. https://doi.org/10.1016/j.asr.2018.03.008.

Kalita, B.R., Bhuyan, P.K., Yoshikawa, A., 2015. NmF2 and hmF2 measurements at 95°E and 127°E around the EIA northern crest during 2010–2014. Earth, Planets Space 67, 186. https://doi.org/10.1186/s40623-015-0355-3.

Kalita, B.R., Bhuyan, P.K., 2017. Variations of the ionospheric parameters and vertical electron density distribution at the northern edge of the EIA from 2010 to 2015 along 95°E and comparison with the IRI-2012. Adv. Space Res. 60 (2), 295–306. https://doi.org/10.1016/j.asr.2016.06.041.

Kil, H., Oh, S.-J., Kelley, M.C., Paxton, L.J., England, S.L., Talaat, E.R., Min, K.-W., Su, S.-Y., 2007. Longitudinal structure of the vertical E × B drift and ion density seen from ROCSAT-1. GeoPhys. Res. Lett. 34, L14110. https://doi.org/10.1029/2007GL030018.

Kil, H., Talaat, E.R., Oh, S.J., Paxton, L.J., England, S.L., Su, S.Y., 2008. Wave structures of the plasma density and vertical E x B drift in low-latitude F region. J. GeoPhys. Res. 113, A09312. https://doi.org/10.1029/2008JA013106.

Lin, C.H., Hsiao, C.C., Liu, J.Y., Liu, C.H., 2007. Longitudinal structure of the equatorial ionosphere: the evolution of the four peaked EIA structure. J. GeoPhys. Res. 112, A12305. https://doi.org/10.1029/2007JA012455.

Liu, H., Watanabe, S., 2008. Seasonal variation of the longitudinal structure of the equatorial ionosphere: does it reflect tidal influences from below? J. GeoPhys. Res. 113, A08315. https://doi.org/10.1029/2008JA013027.

Liu, L., Wan, W., Ning, B., Zhang, M., He, M., Yue, X., 2010. Longitudinal behaviors of the IRI-B parameters of the equatorial electron density profiles retrieved from FORMOSAT-3/COSMIC radio occultation measurements. Adv. Space Res. 46 (8), 1064–1069. https://doi.org/10.1016/j.asr.2010.06.005.

Luhr, H., Xiong, C., 2010. IRI-2007 model overestimates electron density during the 23/24 solar minimum. GeoPhys. Res. Lett. 37, L23101. https://doi.org/10.1029/2010GL045430.

McDonald, S.E., Dymond, K.F., Summers, M.E., 2008. Hemispheric asymmetries in the longitudinal structure of the low-latitude nighttime ionosphere. J. GeoPhys. Res. 113, A08308. https://doi.org/10.1029/2007JA012876.

McNamara, L.F., Retterer, J.M., Baker, C.R., Bishop, G.J., Cooke, D.L., Roth, C.J., Welsh, J.A., 2010. Longitudinal structure in the CHAMP electron densities and their implications for global ionospheric modeling. Radio Sci. 45, RS2001. https://doi.org/10.1029/2009RS004251.

Oberheide, J., Forbes, J.M., 2008. Thermospheric nitric oxide variability induced by nonmigrating tides. GeoPhys. Res. Lett. 35, L16814. https://doi.org/10.1029/2008GL034825.

Sagawa, E., Immel, T.J., Frey, H.U., Mende, S.B., 2005. Longitudinal structure of the equatorial anomaly in the nighttime ionosphere observed by IMAGE/FUV. J. GeoPhys. Res. 110, A11302. https://doi.org/10.1029/2004JA010848.

Scherliess, L., Thompson, D.C., Schunk, R.W., 2008. Longitudinal variability of low-latitude total electron content: tidal influences. J. GeoPhys. Res. 113, A01311. https://doi.org/10.1029/2007JA012480.

Titheridge, J.E., 1995. Winds in the ionosphere—a review. J. Atmos. Terr. Phys. 57, 1681–1714. https://doi.org/10.1016/0021-9169(95)00091-F.

Yu, S., Xiao, Z., Zhao, B., Zhang, D., Hao, Y., 2016. Longitudinal difference in total electron content over the East Asian region: feature and explanation. J. Atmos. Terr. Phys. 148, 74–81. https://doi.org/10.1016/j.jastp.2016.08.015.

Zhang, S.-R., Foster, J.C., Coster, A.J., Erickson, P.J., 2011. East-West Coast differences in total electron content over the continental US. GeoPhys. Res. Lett. 38, L19101. https://doi.org/10.1029/2011GL049116.

Zhang, S.-R., Foster, J.C., Holt, J.M., Erickson, P.J., Coster, A.J., 2012. Magnetic declination and zonal wind effects on longitudinal differences of ionospheric electron density at midlatitudes. J. GeoPhys. Res. 117, A08329. https://doi.org/10.1029/2012JA017954.

Zhao, B., Wang, M., Wang, Y., Ren, Z., Yue, X., Zhu, J., Wan, W., Ning, B., Liu, J., Xiong, B., 2013. East-west differences in F-region electron density at midlatitude: evidence from the Far East region. J. GeoPhys. Res. 118, 542–553. https://doi.org/10.1029/2012JA018235.